Electrochemical Infrared Studies of Monocrystalline Iridium Surfaces. 3. Adsorbed Nitric Oxide and Carbon Monoxide as Probes of Ir(100) Interfacial Structure

Roberto Gómez[†] and Michael J. Weaver*

Department of Chemistry, Purdue University, West Lafayette, Indiana 47907

Received: November 5, 1997; In Final Form: February 3, 1998

The adsorption of carbon monoxide and nitric oxide on Ir(100) in acidic aqueous solutions has been probed by voltammetry together with in-situ infrared reflection−absorption spectroscopy, with the objective of assessing the substrate as well as adlayer structure and bonding. The ordered Ir(100) surface was prepared by flame annealing followed by cooling in a H_2/Ar stream. Similar to, and consistent with, the reported behavior in ultrahigh vacuum (UHV), at potentials $E \geq 0$ V vs SCE (i.e., in the presence of coadsorbed water) the C−O stretch (ν_{CO}) for adsorbed CO occurs at frequencies, 1970−2040 cm^{-1}, that are indicative of atop (or near-atop) surface coordination. At lower potentials where coadsorbed hydrogen is present, however, the ν_{CO} spectra at intermediate CO coverages ($0.2 < \theta_{CO} < 0.5$) include a lower-frequency band suggestive of bridge-bonded CO. The voltammetric features for hydrogen adsorption−desorption, dominated by a sharp current−potential peak at −0.04 V, are consistent with the formation of localized H islands in the presence as well as absence of coadsorbed CO. The ν_{CO} spectral form at intermediate CO coverages, however, indicates that some CO/H intermixing is also present. The occurrence of partial NO dissociative chemisorption is evident from the voltammetry for irreversibly adsorbed layers. This is also consistent with the N−O stretching (ν_{NO}) infrared spectra which exhibit relatively weak bands at frequencies ca. 1620−1650 and 1790−1810 cm^{-1}, suggestive of the presence of bridging as well as atop NO. The infrared spectral as well as the voltammetric findings are diagnostic of the presence of an *unreconstructed* Ir(100) surface by comparison with the reported behavior for the (1 × 1) and hexagonal reconstructed forms of Ir(100) in UHV.

Introduction

A centrally fundamental issue in electrochemical surface science, as for analogous ordered surfaces in ultrahigh-vacuum (UHV) environments, involves elucidating the metal substrate structure in the presence of chemisorbate and other interfacial species. More specifically, the surface atomic structure is known to be affected by chemisorption in that adsorbates can either remove or induce reconstructed phases.[1] While extensive information on such phenomena has been obtained for metal−UHV systems in recent years, especially by using diffraction methods, corresponding insights for electrochemical interfaces are decidedly more limited. Indeed, the direct in-situ observation of electrochemical surface reconstructions originated only with the emergence of scanning tunneling microscopy (STM) and surface X-ray scattering during the present decade,[2,3] although some structural information can be obtained by electrode transfer in UHV.[4] The nature of electrode potential- and adsorbate-induced reconstructions on ordered gold−aqueous interfaces has been examined in detail by both in-situ STM and SXRS.[2,3] However, there remains a severe paucity of such in-situ information for more reactive electrochemical interfaces, most pointedly for ordered Pt-group electrodes given their rich adsorptive and catalytic chemistry. This situation is due partly to the difficulty of maintaining such strongly chemisorbing surfaces free of impurities during in-situ STM and SXRS measurements.

One in-situ microscopic-level probe that is readily applicable to such transition-metal electrochemical interfaces is infrared reflection−absorption spectroscopy (IRAS). As is well documented,[5−8] the use of potential-difference IRAS techniques along with thin-layer solution geometries has spawned an increasing variety of adsorption studies at ordered transition-metal electrodes. One fundamentally stimulating topic involves the chemisorption of simple molecules, especially CO and NO, that have also been probed extensively at ordered metal−UHV interfaces. Such examinations have uncovered interesting similarities and differences in surface structure and bonding within corresponding electrochemical and UHV environments.[2,7−12] The dissimilarities include different binding sites and vibrational band frequencies, which can be traced to the influences of double-layer solvation and surface electronic charge and collectively with differences in the surface potential.[7−11]

We have recently been examining the electrochemical and infrared properties of CO and NO adsorbed at low-index iridium electrodes[13,14] as part of a broader examination of the adsorptive and electrocatalytic properties of ordered iridium− and palladium−aqueous interfaces.[13−15] (References 14 and 13a form parts 1 and 2, respectively, of this series.) The behavior of the Ir(100) surface is of interest from more than one perspective. This metal is known to reconstruct to form a stable (5 × 1) hexagonal ("hex") phase in UHV. The reconstruction is lifted only incompletely upon CO or NO adsorption in UHV even at ambient temperatures,[16,17] which contrasts the (5 × 1) → (1 × 1) transition which is readily induced on Pt(100) under these conditions.[18,19] Furthermore, the coverage-dependent infrared spectral fingerprints for CO and especially NO are decidedly different on the initially unreconstructed (1 × 1) and hex phases of Ir(100).[16b,17] This substrate structure sensitivity provides an

[†] Permanent address: Departament de Química Física, Universitat d'Alacant, Apartat 99, E-03080 Alacant, Spain.

S1089-5647(98)00098-4 CCC: $15.00
Published on Web 04/22/1998

interesting opportunity to utilize IRAS as an in-situ (albeit empirical) monitor of the presence or absence of Ir(100) reconstruction in electrochemical environments.

We describe herein the coverage- and potential-dependent vibrational properties of CO and NO adsorbed at ordered Ir(100)−acidic aqueous interfaces. The Ir(100) surface, prepared by flame annealing and cooling in hydrogen following established procedures,[20] is surmised to be unreconstructed on the basis of the CO, and especially NO, spectral fingerprints in comparison with the UHV behavior. This deduction is also compatible with the voltammetric properties of Ir(100). In addition, the vibrational spectra of CO on Ir(100) exhibit an interesting sensitivity to the electrode potential as well as adsorbate coverage, identified as arising from the presence of coadsorbed hydrogen. The latter findings are similar to the vibrational behavior observed previously on Pt(100),[21a] which is known from STM to be present in a (1 × 1) state.[21b]

Experimental Section

The Ir(100) single crystal (9.5 mm in diameter, 2 mm thick) was purchased from the Material Preparation Facility at Cornell University. It was oriented within ± 1°, as verified by X-ray diffraction. The surface was repolished with diamond paste down to grain size $^1/_4$ μm. The final treatment was flame annealing, by heating the electrode in an oxygen/gas flame at 1500−1700 °C for 15 min, to remove the "devastated" layer formed during the polishing process. Further annealing did not alter the final voltammetric profile. Before each experiment, the crystal was flame-annealed again at 1500−1700 °C for 3−5 s and cooled in a fast-flowing stream of hydrogen and argon, followed by immersion in ultrapure water saturated with these gases (cf. ref 20). The surface was then transferred to the electrochemical or spectroelectrochemical cell while protected by a drop of water.

Electrolytes were prepared from concentrated perchloric acid or sulfuric acid (GFS Chemicals) using ultrapure water (Millipore Milli-Q) and degassed by bubbling argon for at least 10 min. Carbon monoxide-containing solutions were prepared by bubbling CO (AIRCO, grade 2.3) through a previously deaerated solution. To obtain NO adlayers, we employed two different media: either acidic KNO_2 (EM Science)[22] or NO-containing solutions prepared from the pure gas (AIRCO, grade 2.3).

Details of the experimental IRAS measurements are largely as described previously.[23,24] The infrared spectrometer was an IBM (Brucker) IR-98-4A Fourier transform instrument, with a Globar light source and a liquid-N_2 cooled narrow-band MCT detector (Infrared Associates). The spectral resolution was ±4 cm^{-1}. The optical arrangement involved the use of an electrochemical thin layer formed by pushing the disk electrode up to the CaF_2 window. The infrared beam was incident at 60° to the surface normal, with the window beveled at the same angle. Electrode potentials are quoted versus a saturated calomel electrode (SCE). All experiments were performed at room temperature, 23 ± 1 °C.

Results and Discussion

Parts A and B of Figure 1 show typical voltammograms obtained at 50 mV s^{-1} for ordered Ir(100) in 0.1 M $HClO_4$ and 0.1 M H_2SO_4 electrolytes, respectively. The voltammetric morphologies observed with the large iridium crystal employed here are very similar to those reported earlier by using a smaller "Clavilier-type" bead electrode, also cooled in hydrogen after flame annealing.[25] Notable features are the very sharp and reversible spikes observed near 0 V associated with hydrogen adsorption−desorption. In marked contrast to the behavior on most other low-index Pt-group surfaces, the voltammetry obtained in $HClO_4$ and H_2SO_4 electrolytes is intriguingly similar despite the more extensive adsorption expected for sulfate. However, we detected virtually no sulfate (or bisulfate) adsorption on Ir(100) by means of IRAS, whereas strong adsorption is evident on Ir(111) on the basis of an intense potential-dependent S−O stretching band observed in the frequency region 1250−1310 cm^{-1}.[26] [This notable sensitivity of anion adsorption to the crystallographic orientation is qualitatively similar to that observed by IRAS for sulfate on Pt(100) compared to (111).[27]]

The cyclic voltammograms on Ir(100) are extremely symmetric and reproducible in perchloric as well as sulfuric acid as long as the upper potential limit is ca. 0.8 V or below. This behavior indicates an absence of ClO_4^- reduction to Cl^-, contrasting the voltammetric hysteresis observed on Ir(110) in the former electrolyte at low potentials.[13a] However, extending the voltammetric excursions on Ir(100) to higher potentials triggered progressive changes over a number of cycles, as are illustrated in parts A and B of Figure 2 in 0.1 M $HClO_4$ and 0.1 M H_2SO_4, respectively. Specifically, repeated cycling between −0.25 and 1.2 V yielded the gradual growth of voltammetric features in regions a and d and attenuation of the initially pronounced current peaks at b and c (Figures 2A, B). These changes are consistent with the occurrence of oxide-induced surface disordering, similarly to that observed for other Pt-group metals. Significantly, however, they occur on Ir(100) only gradually, requiring a number of voltammetric cycles to develop.

Voltammetric Oxidation of CO Adlayers. Prior to presenting the infrared results, it is useful to consider some voltammetric properties of CO adlayers on Ir(100). Trace a in Figure 3 is an anodic voltammogram at 50 mV s^{-1} for oxidizing adsorbed CO to CO_2. The saturated adlayer was formed at 0.05 V in CO-saturated 0.1 M $HClO_4$, followed by sparging argon so to remove the solution CO. The initial segment of trace a, from 0.05 to −0.25 V and return, shows the expected blocking of H adsorption−desorption by adsorbed CO. The subsequent anodic wave for CO oxidation is followed upon sweeping back from 0.7 to −0.25 V and return (trace b, Figure 3) by voltammetric features identical to those seen prior to CO dosing (Figure 3), indicating the absence of irreversible surface structural changes induced by CO adsorption. Given that CO is known to at least partially lift the hex reconstruction on Ir(100),[16] this provides the first piece of evidence that the Ir(100) surface examined here is *not* reconstructed [i.e., has initially a (1 × 1) structure following flame annealing/hydrogen cooling].

While voltammograms such as in Figure 3 can be used to determine the CO coverage, it is necessary to correct the total charge density, Q_{tot}, contained under the anodic voltammetric wave between electrode potentials E_i and E_+ for the various faradaic and nonfaradaic processes that are coupled to CO oxidative removal.[28−31] The "true" faradaic charge for CO adlayer oxidation, Q_{CO}^{far}, is related to Q_{ob} by[31]

$$Q_{CO}^{far} = Q_{ob} - Q_{dis} - Q_b \qquad (1)$$

Here Q_{dis} is the reverse of the "displacement" charge density measured at a given initial electrode potential E_i upon adsorbing the CO adlayer,[30] and the last term is the "background" voltammetric charge density, Q_b , consumed between E_i and the "anodic limit" potential E_+ (to which Q_{ob} also refers) but

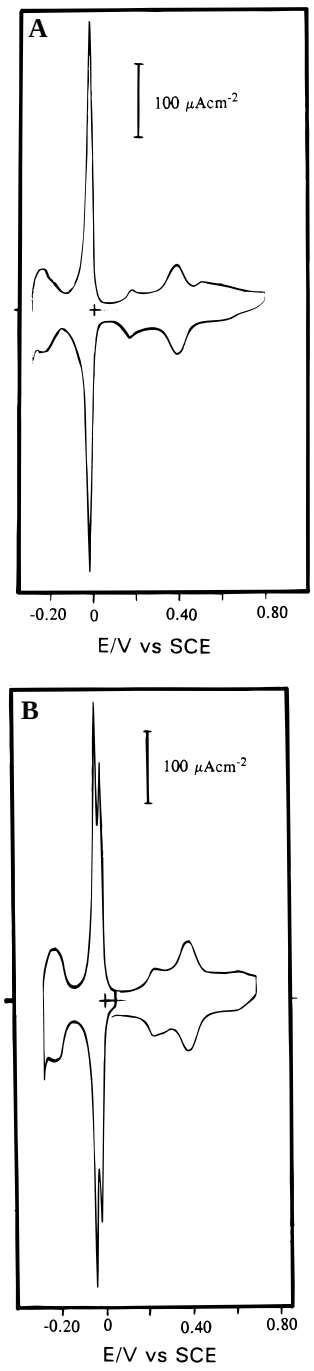

Figure 1. Cyclic voltammograms obtained at 50 mV s^{-1} for ordered Ir(100) in (A) 0.1 M $HClO_4$ and (B) 0.1 M H_2SO_4.

in the absence of adsorbed CO. These two terms ($Q_{dis} + Q_b$) together constitute the required "double-layer" correction to Q^{tot}, enabling an accurate evaluation of Q_{CO}^{far} and hence the CO coverage.[31] As usual,[30] Q_{dis} was obtained from the (reversed-sign) integral of the current−time transient following sudden addition of solution CO;[32] the value 20 μC cm^{-2} was measured at 0.05 V. The Q_b value, 150 μC cm^{-2}, was obtained from the charge flowing between E_i (0.05 V) and E_+ (0.7 V) in the absence of CO. Given that $Q_{ob} = 460$ μC cm^{-2} between the same E_i and E_+ values, one obtains $Q_{CO}^{far} = 290$ μC cm^{-2} from eq 1. Since the metal atomic density of a (1 × 1) Ir(100) surface is 1.35×10^{15} atoms cm^{-2}, and CO oxidation is a two-electron process, we deduce that the saturated fractional CO coverage, θ_{CO}, is 0.65. As for saturated CO adlayers on other Pt-group transition-metal electrodes analyzed by the above method,[31] this

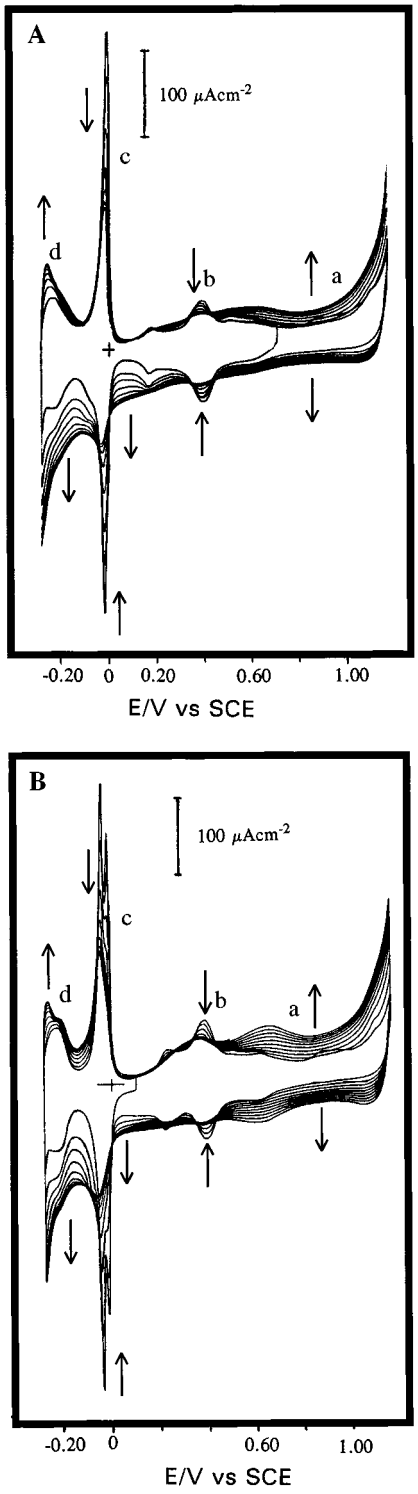

Figure 2. Progressive changes in form of cyclic voltammogram at 50 mV s^{-1} for Ir(100) in (A) 0.1 M $HClO_4$ and (B) 0.1 M H_2SO_4 brought about by selecting higher positive-potential limit, 1.2 V vs SCE.

coulometric θ_{CO} value is close to that, ca. 0.62, extracted by infrared spectrophotometry (vide infra).[28]

Similar to earlier studies on CO adsorption and electrooxidation from this laboratory (e.g., refs 13, 21, 23, and 33), it is useful to examine also voltammetric profiles for oxidizing subsaturated CO adlayers formed by either (A) electrooxidative stripping or (B) direct CO dosing. The former preparative method involves partial electrooxidative removal of an initially saturated adlayer, whereas the latter entails controlled-time (<5 min) dosing up to the desired coverage by using dilute (ca. 10^{-5}

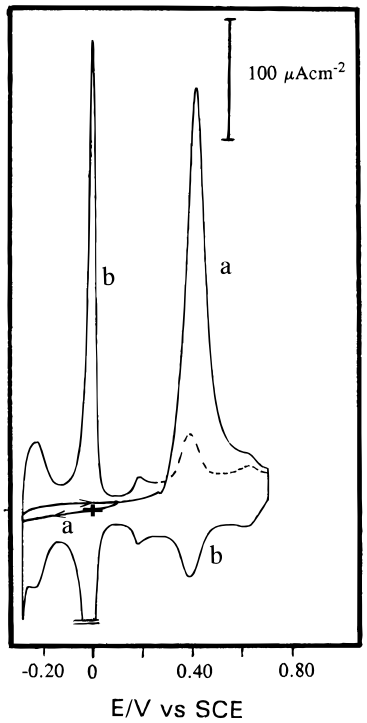

Figure 3. Voltammogram at 50 mV s^{-1} for the oxidation of saturated irreversibly adsorbed CO layer on Ir(100), formed initially at 0.05 V (trace a), and the ensuing cathodic−anodic voltammogram (trace b).

M) CO-containing electrolyte. Parts A and B of Figure 4 show examples of anodic voltammograms obtained for these two types of intermediate-coverage CO adlayers. In the former case, the voltammogram b was obtained immediately after the partial electrooxidation undertaken in trace a. The onset of the anodic wave in b is seen to be shifted slightly to lower potentials yet contains a higher potential shoulder. The partial availability of the surface for hydrogen adsorption−desorption is also evident in the voltammetric segment b. A roughly comparable CO coverage formed by direct CO dosing (Figure 4B) yields similar results, although the *entire* anodic wave for CO oxidation (wave b) is now clearly shifted to lower potentials in comparison with the saturated-adlayer case (Figure 3). This tendency of the directly dosed adlayer to undergo voltammetric oxidation more readily than those formed by partial electrooxidative stripping of a saturated CO layer has been noted on other Pt-group surfaces[21a,33] and is considered further below.

Infrared Spectra of CO Adlayers: Effect of H Coadsorption. Parts A and B of Figure 5 show sequences of θ_{CO}-dependent infrared absorbance spectra obtained on Ir(100) under "electrooxidative stripping" and "direct dosing" conditions, respectively, both at −0.26 V in 0.1 M $HClO_4$. The former set was obtained by forming the saturated irreversibly adsorbed layer and then electrooxidatively removing it in stages by means of short (0.5−2 s) potential pulses to 0.4−0.5 V. Each spectrum involved acquiring 100 interferometer scans, subtracted from which was a "reference" spectrum acquired similarly following complete CO electrooxidation at 0.54 V. The CO coverages indicated alongside each spectrum were determined, as before,[28] from the 2343 cm^{-1} band intensity for the CO_2 thin-layer product appearing in the potential-difference spectra. [The required calibration for this procedure was extracted from the corresponding CO_2 band intensity for saturated adlayer electrooxidation on Pt(110), for which $\theta_{CO} = 1.0$.[28]] The resulted saturated CO coverage, $\theta_{CO} \approx 0.62 \pm 0.03$, is close to the value 0.65 obtained by coulometric means (vide supra) and also

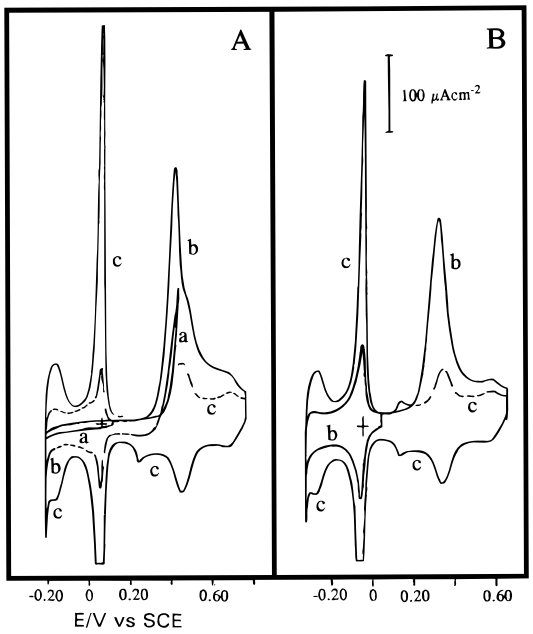

Figure 4. Anodic−cathodic cyclic voltammograms at 50 mV s^{-1} on Ir(100) in 0.1 M $HClO_4$ for intermediate-coverage CO adlayers formed by (A) partial electrooxidative stripping from saturated layer and (B) dosing from dilute (ca. 10^{-5} M) CO-containing solution. Trace a in (A) shows partial adlayer voltammetric removal, immediately followed by remaining adlayer oxidation (trace b) and ensuing cyclic voltammogram for resulting clean surface (trace c). Corresponding traces b and c in (B) refer to removal of dosed intermediate-coverage adlayer.

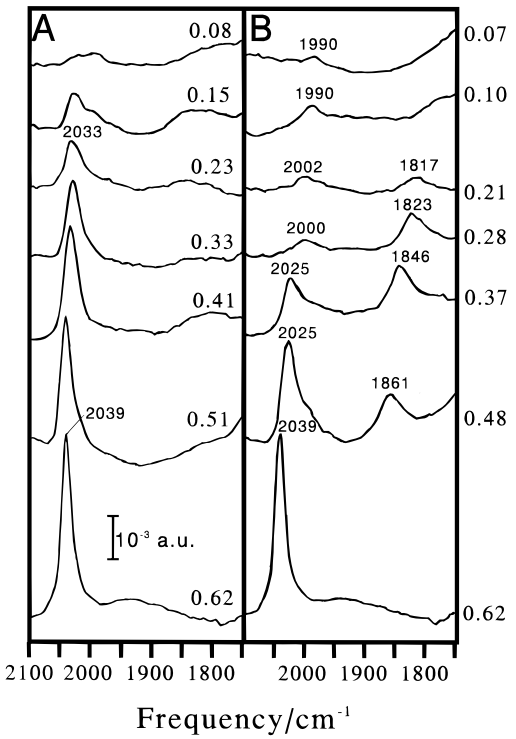

Figure 5. Infrared absorbance spectra obtained in C−O stretching (ν_{CO}) region for sequences of CO coverages (θ_{CO}) indicated on Ir(100) in 0.1 M $HClO_4$ at −0.26 V, formed by (A) partial electrooxidative stripping from an initially saturated ($\theta_{CO} \approx 0.62$) adlayer, and (B) direct dosing up to desired coverage from dilute (10^{-5} M) CO-containing electrolyte. See text for other details.

comparable to the rough estimate of ca. 0.5 for the (1 × 1) Ir(100) surface in UHV at room temperature surmised from low-energy diffraction measurements.[16a] The θ_{CO}-dependent spectra in Figure 5B ("direct-dosing" condition) were obtained, as

above, by exposing the Ir(100) surface to a dilute (10^{-5} M) CO-containing solution for varying time periods (<5 min).

Examination of Figure 5A shows that the spectral form is not altered greatly upon diminishing θ_{CO} by progressive electrooxidative stripping. A single C−O stretching (ν_{CO}) band is seen at 2039 cm^{-1} for the saturated adlayer at −0.26 V (bottom spectrum) which can be attributed on the basis of its relatively high frequency to atop binding (vide infra). This band downshifts only by ca. 10 cm^{-1} or less as θ_{CO} is decreased, although a low-frequency shoulder becomes more pronounced. This type of θ_{CO}-dependent behavior, featuring ν_{CO} intensity diminution with only minor changes in spectral form and frequency, has been observed for CO adlayers on several other low-index Pt-group electrodes.[9,21a,33,34] It is indicative of the formation of large CO islands during electrooxidation, featuring CO removal only at the edges of such close-packed domains by reaction with water or hydroxyl species adsorbed at adjacent sites, so that the local environment (dipole coupling, etc.) is insensitive to the average (macroscopic) CO coverage.[34]

Also, similar to these earlier studies, the ν_{CO} spectra obtained by forming a given coverage by dilute CO solution dosing exhibit markedly greater changes with increasing θ_{CO} (Figure 5B). However, the nature of the present θ_{CO}-dependent spectra is somewhat unusual. At the lowest coverages, $\theta_{CO} < 0.2$, a single ν_{CO} band is observed at around 1990 cm^{-1}. The ca. 50 cm^{-1} lower frequencies compared to that for the saturated CO adlayer can be attributed primarily to markedly diminished dipole−dipole coupling at low coverages, similar to that observed on several Pt-group electrochemical surfaces as well as in UHV.[8,9,21,23,33,34] Increasing the coverage above 0.2 yields an additional ν_{CO} band at 1815−1860 cm^{-1}, the frequency upshifting with θ_{CO} (Figure 5B). We tentatively ascribe this feature to "bridging CO" on the basis of its 150−200 cm^{-1} lower frequency compared with the "atop" ν_{CO} band. (One should nonetheless bear in mind the recently demonstrated ambiguities in assigning binding sites purely on the basis of vibrational frequencies.[35]) The observation of such lower-frequency ν_{CO} features on low-index iridium surfaces is noteworthy in that all three low-index faces in UHV yield only a *single* ν_{CO} band at frequencies in the range 2000−2100 cm^{-1}.[16,36] [The Ir(111) and (110) electrochemical surfaces behave in a fashion largely similar to the UHV systems in this respect.[13a,37]] Moreover, increasing the dosed CO coverage on Ir(100) further, above 0.5 up to saturation ($\theta_{CO} = 0.62$), yields a complete *reversion* of the binding geometry back to atop CO in that the lower-frequency ν_{CO} band is removed entirely and replaced by the higher-frequency feature (Figure 5B). Consequently, then, the θ_{CO}-dependent ν_{CO} band morphology is notably nonmonotonic at low potentials, the "bridging" feature appearing under dosing conditions only at intermediate coverage, at −0.26 V, for $0.2 < \theta_{CO} < 0.5$.

Insight into the likely factor(s) responsible for this unusual θ_{CO}-dependent ν_{CO} behavior is obtained by examining the ν_{CO} spectra for various dosed coverages as a function of electrode potential, *E*. Figure 6 shows representative sets of such $\nu_{CO}-E$ data for low, intermediate, and saturation dosed θ_{CO} values, 0.09, 0.30, and 0.62. These data were obtained by stepping the potential to the values indicated, starting from −0.26 V, acquiring 100 interferometer scans at each potential before obtaining a "reference spectrum" (as before) at 0.5 V after the adlayer was completely electrooxidized. A notable aspect of Figure 6 is the *complete loss* of the "bridging" ν_{CO} band at the intermediate coverage upon altering the potential above 0 V, accompanied by a marked intensity increase in the "atop" ν_{CO}

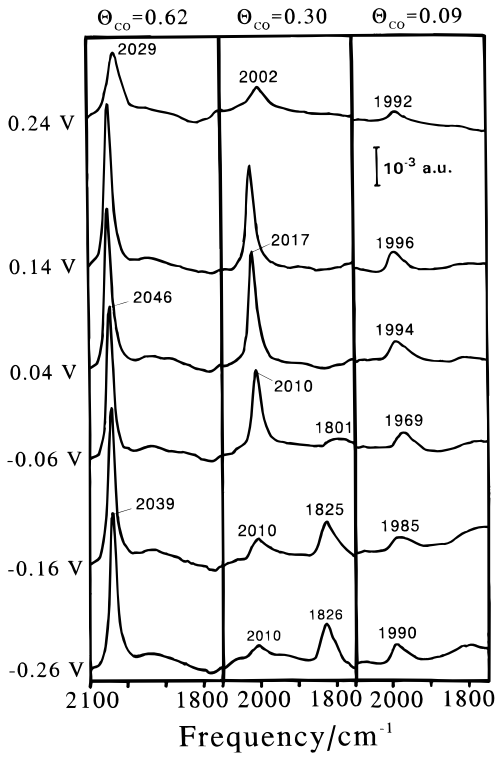

Figure 6. Electrode potential-dependent ν_{CO} spectra for three dosed CO coverages, as indicated, on Ir(100) in 0.1 M $HClO_4$. See text for other details.

feature. The ν_{CO} spectra were found to be sensitive only to the CO coverage and electrode potential, rather than on the previous potential-dependent history following adlayer formation. Thus, the θ_{CO}-dependent spectra obtained by CO dosing at potentials above 0 V exhibit only the atop ν_{CO} band, and the bridging ν_{CO} band appears at intermediate coverages upon altering the potential to values below 0 V. This behavior is quite distinct from that reported previously for CO dosed on Ir(111), where spectral disparities were found following adlayer formation at different electrode potentials and subsequent alteration of the potential to a common value.[36]

Comparing the *E*-dependent ν_{CO} spectra for $\theta_{CO} = 0.3$ in Figure 6 with the voltammetric traces for hydrogen desorption is instructive. In the presence of an intermediate-coverage CO adlayer as well as in the absence of CO (curves b and c, respectively, Figure 4), the adsorbed hydrogen is removed over a narrow potential range, within −0.15 to 0.05 V. Significantly, the *E*-dependent ν_{CO} spectra reveals that the removal of the "bridging" ν_{CO} feature along with the intensity increase in the "atop" band occurs within exactly the same potential region. This point is clarified by inspecting sets of *E*-dependent ν_{CO} data obtained for intermediate dosed CO coverages over this relevant potential range, as exemplified in the sequence shown (for $\theta_{CO} = 0.37$) in Figure 7. The intimate correlation between the potential-sensitive removal of chemisorbed hydrogen and the occurrence of bridging/atop CO site conversion is clearly evident upon comparing these spectral data with the voltammetric profiles in Figure 4.

Consequently, then, coadsorbed hydrogen influences markedly the coverage-dependent CO adlayer structure. A significant related, if less dramatic, effect is also evident from Figure 6 at low ν_{CO} coverages. Examination of the *E*-dependent ν_{CO} data for $\theta_{CO} = 0.09$ shows that the band frequency *decreases* with increasing electrode potential in the region, ≤ 0 V, where H desorption is taking place, before upshifting toward more

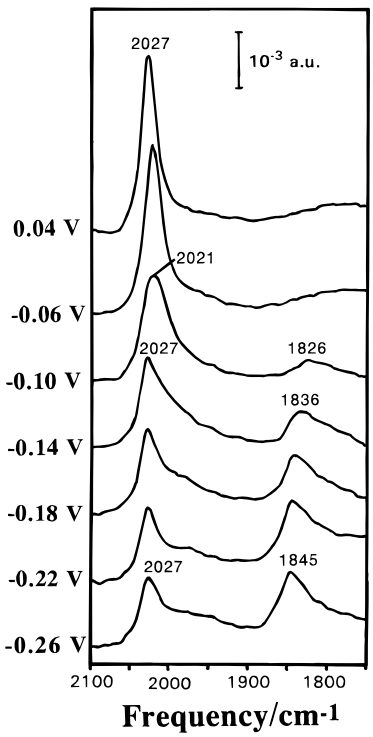

Figure 7. *E*-dependent ν_{CO} spectra for adsorbed CO (dosed coverage = 0.37) on Ir(100) in 0.1 M $HClO_4$, over potential region where CO binding site change is observed.

positive potentials in the range, ca. 0 to 0.2 V, where water rather than hydrogen is the predominant coadsorbate. Indeed, the higher frequency ν_{CO} band partner observed at intermediate CO coverages also shows a similarly nonmonotonic ν_{CO} frequency−potential dependence in the region where the potential-induced site conversion is taking place, as is seen clearly in Figure 7. Such behavior contrasts the usual near-linear *E*-induced upshift in the ν_{CO} frequency which is observed in the present case for the saturated CO adlayer (Figure 6), for which $d\nu_{CO}/dE = 35\ cm^{-1}\ V^{-1}$. (Note that the ν_{CO} frequencies in Figure 6 decrease slightly by 0.24 V, which is due to the onset of slow adlayer electrooxidation by this point.) A similarly nonmonotonic ν_{CO} frequency−*E* dependence has also been observed for "atop" CO at lower coverages on Pt(100) in 0.1 M $HClO_4$.[21] Indeed, the Pt(100)/CO electrochemical interface also yields θ_{CO}-dependent ν_{CO} spectra that exhibit similarities to the present Ir(100) system, especially in their sensitivity to the presence of coadsorbed hydrogen versus water.[21] These and related issues are discussed further below.

Comparison with Coverage-Dependent Infrared Spectra in UHV. Given that the so-called "double-layer" region, above ca. 0 V, where water rather than hydrogen constitutes the major coadsorbate, yields only a single "atop" ν_{CO} band throughout the CO coverage range (Figure 6), it is instructive to compare the θ_{CO}-dependent ν_{CO} frequencies with corresponding vibrational data for the Ir(100)/CO system in UHV.[16] As already mentioned, the latter system also displays exclusively "atop" ν_{CO} bands. Two UHV-based studies have been reported at 300 K, using electron energy loss spectroscopy (EELS)[16a] and IRAS,[16b] both focusing on the form of θ_{CO}-dependent ν_{CO} spectra on the unreconstructed (1 × 1) versus the hexagonal reconstructed (5 × 1) surfaces. While the EELS study found only minor differences in the $\nu_{CO}-\theta_{CO}$ spectra on the (1 × 1) and (5 × 1) substrate,[16a] the higher resolution afforded by IRAS uncovered significant differences in the θ_{CO}-dependent ν_{CO} band shape as well as frequency.[16b] On the (1 × 1) surface, a single ν_{CO} band was observed throughout the range of CO exposures, shifting from 2026 to 2071 cm^{-1}.[16b] (Although θ_{CO} values were not reported in ref 16b, the latter ν_{CO} frequency refers to a saturated adlayer.) On the (5 × 1) surface, however, multiple ν_{CO} bands were observed at low and intermediate CO exposures, yielding a saturated CO adlayer having a higher ν_{CO} frequency, ca. 2095 cm^{-1}. The ν_{CO} peak components are separated by 10−20 cm^{-1} so to be readily resolvable by IRAS but not by EELS.[16] The removal of the (5 × 1) reconstruction, as sensed by LEED, was incomplete even at high CO exposures.[16b]

In comparing these coverage-dependent ν_{CO} data with the present results, as outlined in earlier studies (e.g., refs 8, 9, 21a, 33, 39, and 40), it is instructive to account for differences in the ν_{CO} frequencies between the corresponding electrochemical and UHV-based Ir(100)/CO systems arising from dissimilarities in the effective "surface potential" $\Delta\phi$ (or, equivalently, in the work function, $\Delta\Phi$) between these two interfacial environments. The potential dependencies of the ν_{CO} frequency (the so-called "Stark-tuning" effect[37,38]) for a given adlayer coverage (and structure), $d\nu_{CO}/dE$, can readily be evaluated (vide supra). Consequently, finding significant ν_{CO} differences between the electrochemical and UHV systems after correcting for the surface-potential differences signals the occurrence of intrinsic differences in the adlayer structure and bonding in these two environments.

The required relation between the electrode potential E^M measured for a given interface (vs a reference electrode) and the corresponding work function Φ^M (vs vacuum) is given by[41]

$$E^M = \Phi^M/e - E_k \qquad (2)$$

where E_k is the so-called "absolute" potential of the reference electrode. Taking the E_k value for the standard hydrogen electrode (SHE) to be 4.6 ± 0.2 V,[42] and given that Φ^M for a clean Ir(100) surface is about 5.7 eV,[43] the latter should have a "surface potential" (on the SCE scale) of ca. 0.8 V. Although $\Delta\Phi$ values arising from CO adsorption on Ir(100) have apparently not been determined, the small positive values reported (for saturated adlayers) on Ir(111) and (110), 0.15−0.25 eV, along with similarly small values for other Pt-group metals involving primarily atop CO binding, suggest that a comparable $\Delta\Phi$ estimate, say 0.2 eV, is not unreasonable for Ir(100)/CO.

This analysis applied to the saturated adlayer, given that $d\nu_{CO}/dE \approx 30 \pm 4\ cm^{-1}\ V^{-1}$, yields a ν_{CO} frequency at the appropriate Φ^M value (5.9 eV) of about 2075 cm^{-1}. This ν_{CO} value is close to that measured for a saturated CO adlayer at the (1 × 1) Ir(100) UHV interface, 2071 cm^{-1},[16b] but lower than the frequency for the (5 × 1) surface, ca. 2095 cm^{-1}.[16b] The $d\nu_{CO}/dE$ value in the low-θ_{CO} limit is not known reliably since the hydrogen-free potential range, 0−0.2 V, is restricted. Nonetheless, one anticipates from the behavior of the Ir(110)/CO and Ir(111)/CO systems that feature only atop CO binding that[13a,37] $d\nu_{CO}/dE \sim 50\ cm^{-1}\ V^{-1}$. Extrapolating the electrochemical ν_{CO} frequencies for $\theta_{CO} = 0.09$ on this basis to the appropriate Φ^M value (5.7 eV), again employing eq 2, yields a "low-θ_{CO}" ν_{CO} frequency of ca. 2040 cm^{-1}. While this electrochemical ν_{CO} estimate is slightly higher than the corresponding measured UHV value, ca. 2025−2040 cm^{-1}, the comparison is hampered by uncertainties in the $\nu_{CO}-E$ extrapolation and (unknown) differences in CO coverage.

We can therefore conclude that the θ_{CO}-dependent ν_{CO} behavior at the Ir(100) electrochemical interface within the "double-layer" potential region, involving coadsorbed water, is compatible with the corresponding ν_{CO} spectral characteristics

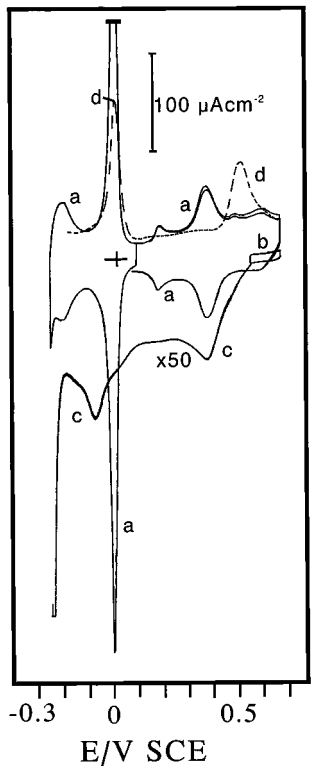

Figure 8. Cyclic voltammetry for Ir(100) in 0.1 M $HClO_4$ before (trace a) and following (traces b−d) irreversible NO adsorption. Sweep rate is 50 mV s^{-1}, except for reduction trace c which refers to 1 mV s^{-1} (with a 50-fold expanded current scale.)

for the (1 × 1) surface in UHV. While one certainly cannot conclude that the present Ir(100) surface also has a (1 × 1) structure merely on this basis, the electrochemical ν_{CO} spectral frequencies and, perhaps more pointedly, the single-peaked band shapes (e.g., Figure 6) are distinctly more compatible with the presence of such an unreconstructed surface than a hexagonal reconstructed one. More persuasive evidence along these lines, however, is obtained from the voltammetric and infrared spectral fingerprints for adsorbed NO, which we now consider.

Voltammetry of NO Adlayers. As for the CO adlayer data, prior to describing the IRAS results for NO adsorption on Ir(100), it is instructive to consider some related voltammetric responses. Two key behavioral differences between adsorbed NO and CO should be borne in mind. First, adsorbed NO is oxidized in acidic media only at high potentials (ca. 1 V vs SCE) to form nitrate and reduces below 0 V yielding ammonium ions.[13,22] The identity of these products on Ir(110) and (111) has been confirmed by potential-difference IRAS.[13] Second, NO adsorption on some Pt-group transition metals, including iridium, can be dissociative even at ambient temperatures in UHV, therefore yielding adsorbed O and N fragments (O_{ad}, N_{ad}) as well as molecular NO.[17,45] Indeed, the formation of O_{ad} on a polycrystalline Ir film electrode from NO adsorption in 0.1 M $HClO_4$ has been observed directly by means of surface-enhanced Raman spectroscopy (SERS).[46] Interestingly, while only molecularly adsorbed NO is present on (5 × 1) Ir(100) in UHV at room temperature, extensive NO dissociation occurs under these conditions on the (1 × 1) surface.[17] As we will see below, this and other behavioral differences between NO adsorption on the (5 × 1) and (1 × 1) substrates provide opportunities for surface structural identification based on both voltammetry and infrared spectroscopy.

Figure 8 summarizes reductive voltammetry obtained following irreversible NO adsorption on Ir(100) in 0.1 M $HClO_4$. The freshly annealed Ir(100) surface was first immersed in NO-saturated 0.1 M $HClO_4$ for 1 min, then rinsed with ultrapure water, and transferred to the electrochemical cell containing argon-purged 0.1 M $HClO_4$. The electrode was immersed at 0.7 V, where NO is stable to both reduction and oxidation. The initial narrow voltammetric cycle (at 50 mV s^{-1}) between 0.65 and 0.55 V (trace b) shows that the current flowing in this region for clean Ir(100) is largely blocked. (Trace a is a voltammogram for an NO-free electrode.) A negative-going potential sweep at 1 mV s^{-1}, initiated at 0.57 V, is shown as trace c in Figure 8. (The current scale for trace c is expanded 50 times to compensate for the smaller sweep rate.) A pair of cathodic peaks at 0.4 and −0.1 V are evident in trace c. While the latter is located at a potential consistent with NO reduction to NH_4^+, as is observed for similar conditions on Ir(110) and (111),[13] the position of the former peak is suggestive instead of reduction of O_{ad} or related oxygenated species (such as OH_{ad}).

A rough estimate of the total coverage of these species, θ_t (such as $NO_{ad} + O_{ad} + N_{ad}$), can obtained from the combined charge under these cathodic features, Q_t. The Q_t value between 0.57 and −0.21 V, corrected for "double-layer charging", is about 600 μC cm^{-2}. The charge consumed by the coupled formation of hydrogen, 120 μC cm^{-2}, was obtained from the area under peak d observed during the ensuing positive-going sweep at 50 mV s^{-1}. Assuming an "overall" five-electron reduction (i.e., presuming that the chemisorbed species together form NH_4^+ or H_2O) yields a θ_t value of ca. 0.45. From the peak morphology of trace c, roughly half of this total chemisorbate coverage appears to be present as molecularly adsorbed NO. The implied occurrence of partial NO dissociation on the present Ir(100) surface differs from the behavior of Ir(110) and (111) in acidic electrolytes, for which the close-packed adsorbate coverages extracted from cathodic and anodic voltammetry (as well as from the infrared spectra) are indicative of the presence of near-exclusive *molecular* NO adsorption.[13]

Voltammograms obtained upon repeated potential cycling of such irreversibly adsorbed layers on Ir(100) provide further evidence for the formation of additional redox-active adsorbates besides NO. Figure 9A shows cathodic−anodic voltammograms obtained at 50 mV s^{-1} after transfer of an irreversibly adsorbed adlayer to 0.1 M $HClO_4$. Widening the potential "window" to successively lower values while maintaining the upper limit at 0.7 V, as depicted in traces a−c in Figure 9A, shows the progressive emergence of an anodic feature at 0.55 V as well as cathodic peaks at about 0.4 and 0.15 V. Repeated cycling between 0.7 and 0.05 V yielded a stable voltammetric profile containing these peaks. Comparable voltammetric behavior under such conditions has also been observed for irreversibly adsorbed NO on Pt(100) and attributed tentatively to the formation of a chemically reversible redox couple (or couples) involving adsorbed HNO species.[47] Significantly, transferral of the Ir(100) electrode exhibiting this voltammetric profile to the IRAS cell yielded no detectable N−O stretching (ν_{NO}) bands (vide infra), indicating further that the redox-active adsorbate is formed by decomposition of adsorbed NO. Expanding the voltammetric window further, so to cycle between 0.7 and −0.25 V (Figure 9B), yielded slow removal of the aforementioned current peaks and eventual recovery of the usual voltammetric profile for clean Ir(100) in 0.1 M $HClO_4$.

Regardless of such details, the deduction from voltammetry that extensive NO dissociation occurs at the present Ir(100)−aqueous interface, together with the UHV-based behavior mentioned above, provides a further indication that the substrate is not reconstructed. The strongest evidence for this conclusion,

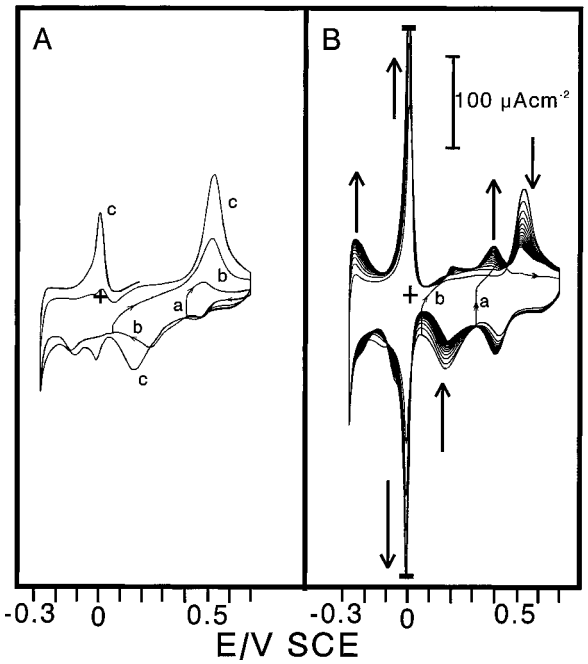

Figure 9. Voltammograms obtained at 50 mV s^{-1} during repeated potential cycling of irreversibly adsorbed NO layers on Ir(100) in 0.1 M $HClO_4$. (A) Effect of decreasing lower potential limit for fresh adlayer. (B) Progressive voltammetric changes induced by subsequent repeated cycling between 0.7 and −0.25 V.

however, is obtained from the IRAS data for NO, which is described next.

Infrared Spectra of NO Adlayers: Implications for Substrate Structure. As alluded to above, a previous detailed IRAS study of NO adsorption on Ir(100) surfaces in UHV uncovered notable differences in the N−O stretching (ν_{NO}) spectral fingerprint depending if the surface structure was initially (1 × 1) or (5 × 1).[17] Adsorption on the latter surface yields dominant ν_{NO} bands around 1815−1850 cm^{-1} at 300 K (attributed tentatively to "atop" NO); NO dissociation does not commence until higher temperatures. In contrast, NO adsorption on the (1 × 1) surface produces a dominant lower-frequency ("bridging") feature in addition to the "atop" ν_{NO} band. While the appearance of these spectral features on the (1 × 1) surface requires high NO exposures at 300 K since extensive NO dissociation occurs at lower dosages, similar differences in the ν_{NO} spectral fingerprint with that seen on the (5 × 1) substrate were seen even at lower temperatures (ca. 100 K) where adsorbate dissociation is largely absent.[17] Similarly to the CO case (vide supra), NO adsorption on (5 × 1) Ir(100) does not lift the reconstruction completely even at high NO dosages at 300 K. By analogy, then, the ν_{NO} spectral fingerprint observed for the present ordered Ir(100) electrode should provide a relatively clear-cut, if empirical, probe of the substrate atomic configuration.

Figure 10 shows a potential-dependent set of ν_{NO} infrared spectra for irreversibly adsorbed NO on Ir(100) in 0.1 M $HClO_4$, obtained with this objective in mind. Similar to the voltammograms described above (Figures 8 and 9), the Ir(100) surface was first immersed in NO-saturated 0.1 M $DClO_4$ in D_2O at 0.7 V and then transferred to an NO-free electrolyte. (Deuterated solvent was employed here so to facilitate observation of lower-frequency ν_{NO} bands within the range 1600−1700 cm^{-1} which would be obscured somewhat if H_2O solvent was used.) The *E*-dependent spectral sequence in Figure 10 was obtained for the series of increasingly positive potentials (0.34−0.94 V) indicated, 100 interferograms being acquired at each point before

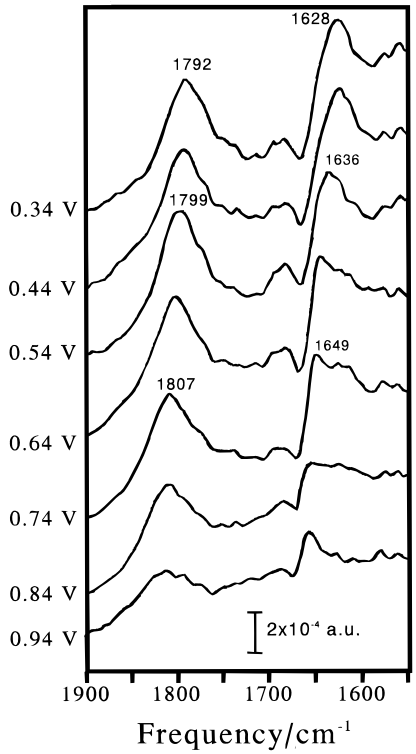

Figure 10. Electrode potential-dependent ν_{NO} infrared spectra for irreversibly adsorbed NO adlayer on Ir(100) in 0.1 M $DClO_4$ in D_2O (formed by immersion into NO-saturated electrolyte) for a series of increasing potentials as indicated. See text for other details.

stepping to 1.14 V to record the "reference spectrum" upon completion of NO electrooxidation. Note that the lower potential limit was chosen to be above the value where NO adlayer reduction occurs, but negative of the 0.4 V cathodic voltammetric feature in Figure 8 (trace c), attributed tentatively to O_{ad} reduction (vide supra).

Examination of Figure 10 reveals a distinct lower-frequency ν_{NO} band at ca. 1630−1650 cm^{-1} with an additional feature at 1790−1810 cm^{-1}. As usual, both these ν_{NO} bands upshift in frequency toward higher potentials and are progressively attenuated by 0.9 V or so, as expected from NO adlayer electrooxidation. The combined intensity of these two features is markedly (3−4-fold) smaller than that for the "atop" NO band at ca. 1800−1830 cm^{-1} observed for a saturated NO layer on Ir(110) in 0.1 M $HClO_4$.[13a] Since the latter case refers to an essentially molecularly adsorbed layer,[13a] this observation lends support to the above deduction from voltammetry that the NO coverage on Ir(100) is substantially below that corresponding to a close-packed NO layer, as a consequence of partial chemisorbate dissociation. Figure 11 shows a similar *E*-dependent ν_{NO} sequence, obtained instead for Ir(100) in NO-saturated 0.1 M $DClO_4$ in D_2O solvent. In this case, the spectral sequence started at 0.64 V for the decreasing *E* values indicated, before obtaining a "reference spectrum" at −0.25 V following adlayer electroreduction. The potential-dependent ν_{NO} fingerprints in Figure 11 are closely similar to those for the irreversibly adsorbed adlayer in Figure 10, again exhibiting both "bridging" and "atop" ν_{NO} bands of comparable intensity.

As in earlier studies,[13,22,46] NO adlayers could be formed on Ir(100) in acidic nitrite as well as NO-saturated solutions, although the NO coverages are apparently lower in the former case. Figure 12 shows a representative *E*-dependent ν_{NO} sequence obtained for Ir(100) in 0.1 M $DClO_4$ (in D_2O) containing 10 mM $NaNO_2$. As in Figure 10, the solvent and

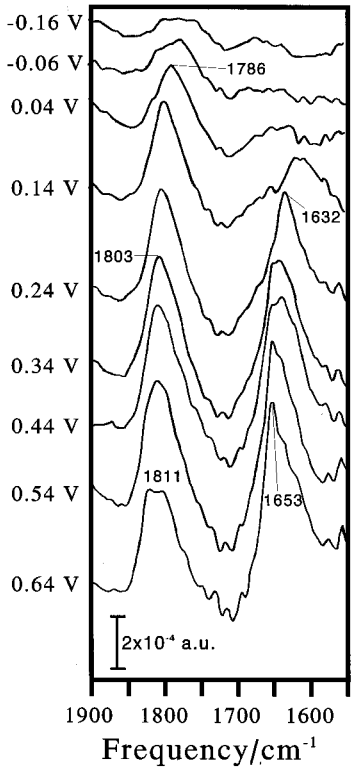

Figure 11. Electrode potential-dependent ν_{NO} spectra for Ir(100) in NO-saturated 0.1 M $DClO_4$ in D_2O for the series of decreasing potentials indicated. See text for other details.

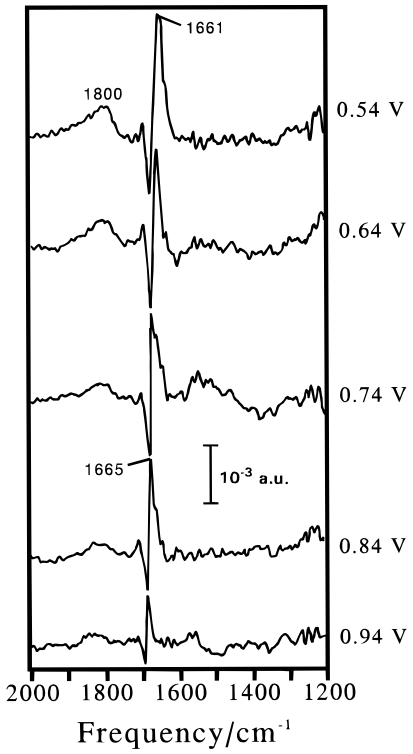

Figure 12. Electrode potential-dependent ν_{NO} spectra for Ir(100) in 0.1 M $DClO_4$ (in D_2O) containing 10 mM $NaNO_2$ at series of increasing potentials indicated. (The negative-going ν_{NO} band component is due to adsorbed NO remaining in the "reference spectrum", obtained subsequently at 1.14 V.) See text for other details.

other spectral interferences were removed by obtaining subsequently a "reference spectrum" at 1.14 V. The ν_{NO} spectra in Figure 12 show a clear "bridging" band at 1650−1680 cm^{-1} between 0.54 and 0.84 V, comparable to (yet more intense than) that seen in Figures 10 and 11, although the higher-frequency ("atop") component at ca. 1850 cm^{-1} is relatively weak and ill-defined. (The negative-going component of the former arises from incompletely oxidized NO at 1.14 V.) This behavior is comparable to that seen for moderate NO exposures on (1 × 1) Ir(100) in UHV at 300 K, where the lower-frequency ν_{NO} component also tends to predominate.[17]

Most importantly, the overall ν_{NO} fingerprints seen in Figures 10−12 for NO adsorbed at the present ordered Ir(100) electrochemical interface are closely similar to those observed by IRAS (and EELS) for NO adsorption on the (1 × 1) Ir(100) surface in UHV, yet *distinctly different* to the spectral form seen for the (5 × 1) surface under similar conditions, including the same (ambient) temperature as employed here.[17] This finding therefore provides strong evidence that the ordered Ir(100) electrochemical surface, at least when prepared by the flame annealing−hydrogen cooling procedure employed here, is present in an initially (1 × 1), *i.e., unreconstructed*, state, rather than the alternative hexagonal reconstructed form. Such a conclusion is also in harmony with the aforementioned, albeit less persuasive, evidence based on the ν_{CO} spectral fingerprint, together with the independent deduction made from the voltammetry of NO adlayers as discussed in the preceding section. In addition, Attard has reached the same conclusion for Ir(100) prepared by a similar flame annealing−hydrogen cooling protocol, also displaying voltammetric profiles as in Figure 1B, by transferring the surface into UHV and observing a (1 × 1) LEED pattern.[48] While such ex-situ procedures can face ambiguities from possible changes in surface structure during the transfer into UHV, the data nevertheless support the validity of the present conclusion from in-situ measurements.

Further Structural Implications. An intriguing feature of the present results is the clear connection established between the presence of coadsorbed hydrogen, observed below 0.05 V (Figure 4B), and the formation of "bridging" as well as "atop" CO as gleaned from the lower-frequency ν_{CO} feature (Figures 5−7). The coadsorption of atomic hydrogen and CO has been examined in some detail on a number of low-index transition metals in UHV.[49] While this coadsorption system on Ir(100) in UHV has apparently not been studied, the general trends established for other (100) faces suggest that microscopically intermixed CO/H adlayers are to be expected on such "open" surfaces.[49] Thus, H/CO coadsorption on Rh(100) in UHV, for example, can yield intermixed adlayers as well as locally separated adsorbed H and CO domains, depending on the relative coverages, dosing sequences, and temperature.[50,51]

Evidence for the presence of microscopically intermixed (as opposed to segregated) H/CO domains from surface vibrational spectroscopy is based primarily on the detection of spectral features, and hence binding sites and/or local interadsorbate interactions, for the coadsorbed system which are absent for the single-component adlayers. Such spectral changes should be distinct from those brought about by coadsorbate-induced "compression" of pure adlayer domains so to yield locally higher packing densities. The latter effect is apparently operative in the Pt(111)/CO,H system in UHV, for example, where CO "compression" structures having locally higher coverages are evident from the IRAS fingerprint for dilute CO adlayers with coadsorbed H, in particular the appearance of a "bridging" ν_{CO} feature.[52] However, even for this supposed "segregated" coadsorbate system,[49] the ν_{CO} spectral features for the mixed H/CO layer, such as the atop ν_{CO} frequency, deviate markedly from those observed for higher-θ_{CO} pure CO adlayers, underscoring the importance of local H/CO interactions.[52]

The ν_{CO} spectral properties of the present Ir(100)/CO,H system support the occurrence of local coadsorbate intermixing. Most pointedly, the observation of bridging as well as atop CO adsorption *only* at intermediate coverages, $0.2 < \theta_{CO} < 0.5$, is only readily interpretable by postulating at least *some* H/CO intermixing. The simple H-induced compression of CO domains, so to yield higher local CO coverages, should yield purely atop CO binding on the basis of Figures 5−7. The H coadsorption-induced formation of bridging CO has also been observed from vibrational spectra in the Rh(100)/CO,H system in UHV and interpreted in terms of local H/CO intermixing.[51] A related observation has also been made on the basis of IRAS data for the Pt(100)/CO,H electrochemical system in acidic aqueous solution.[21a]

Consideration of the voltammetric data for H adsorption−desorption in 0.1 M $HClO_4$ (Figures 1A, 3, and 4), however, yields a somewhat different perspective. As mentioned above, the voltammetry for adsorbed H in 0.1 M $HClO_4$ and H_2SO_4 is remarkedly similar, the former electrolyte yielding a dominant current peak at ca. −0.04 V vs SCE, along with a broader feature at about −0.2 V. The sharpness of the former feature, characterized by a full width at half-maximum (fwhm) of only 25 mV, indicates the presence (at least formally) of *attractive* H−H interadsorbate interactions. [Note that voltammetric peaks associated, as here, with a potential-dependent one-electron equilibrium, having fwhm values below 100 mV (at 25 °C) signal the presence of an adsorption isotherm having an attractive interaction parameter.[53]] Such sharp voltammetric peaks for H on low-index iridium electrodes have been attributed to the occurrence of Ir−H covalent bonding.[25c] Given the observed anion insensitivity of the voltammetric behavior, however, the sharp peaks are most simply accounted for by the formation of H adsorbate islands stabilized by net repulsive interactions with surrounding inner-layer water molecules.

This implied formation of segregated H islands is also consistent with some ν_{CO} spectral as well as voltammetric data in the presence of dosed coadsorbed CO. The latter, as exemplified by trace b in Figure 4B, exhibit the characteristic reversible H adsorption−desorption peak which is attenuated, as expected, but with a shape and position that is *almost unaffected* by the presence of coadsorbed CO. This behavior indicates that the coverage-dependent thermodynamic stability of the adsorbed H (or at least that associated with the −0.04 V voltammetric peak) is not altered discernibly by the presence of CO. Most likely, then, the adsorbed H is present largely as islands that are spatially separated from, and therefore having properties largely unaffected by, the coadsorbed CO. Also consistent with this interpretation is the significant H-induced upshifts in the atop ν_{CO} frequencies at low θ_{CO} values as gleaned from the potential-dependent spectra in the region (≤0 V) where hydrogen coadsorption occurs (Figure 6, far right column). Following the above discussion, this spectral effect is consistent with the compression of CO into "patches" having higher local coverages (and hence increased dipole−dipole coupling) in the presence of the H islands.

Remaining to be explained in this otherwise self-consistent picture, however, is the H-induced appearance of "bridging" CO at intermediate θ_{CO} values. One possibility is that the adsorbed CO forms small (≤nanoscale) domains, which feature a large population of CO's on the island perimeters, and hence adjacent to coadsorbed hydrogens. This adsorbate, perhaps along with CO imbedded in H-rich domains, may well be induced to bind in a bridging rather than atop site. A comparable H-induced binding-site shift for CO on Rh(100) in UHV has been observed upon H_2 postdosing and received a similar interpretation.[51a] Some elements of this picture probably also apply to the Pt(111)/CO,H system mentioned above. Taken together, then, the present findings oblige one to consider more complex adlayer structural models than the (likely oversimplified) "intermixed" and "segregated" pictures that are commonly invoked. It is worth emphasizing that the voltammetric data, especially for the present system, provide uniquely detailed information on the coverage-dependent energetics of hydrogen coadsorption with water and/or CO. It would therefore be of interest to explore this electrochemical coadsorption system in greater detail.

The other noteworthy issue arising from the present investigation concerns the value of vibrational spectroscopy as a probe of substrate structure. In some respects, the present Ir(100)/NO system represents an unusually clear-cut example of the utility of IRAS for elucidating metal substrate structure. This favorable situation arises from the previously demonstrated sensitivity of the ν_{NO} spectral fingerprint to the absence or occurrence of hexagonal reconstruction,[17] connected in part with the stability of the hex surface even in the presence of high NO coverages at ambient temperatures. As a consequence, adsorbed NO acts as a largely "inert" probe of substrate structure, in contrast to the more common situation where even low coverages of NO (or CO) are sufficient to lift entirely the reconstruction, for example on Pt(100).[54] The structural diagnosis is aided further by the markedly greater tendency of the (1×1) Ir(100) surface to dissociate NO in comparison with the hex form. Such NO dissociation in the present case can be gleaned from both the form of the voltammetry and the infrared spectra.

Nevertheless, it is clearly of paramount importance to acquire more direct in-situ information on the atomic (and nanoscale)-level spatial structure of ordered transition-metal electrodes, as can be obtained in favorable cases by both STM and SXRS. An interesting example of the latter approach, specifically to Pt(110), has recently been reported.[55] Such explorations utilizing the former technique, especially to surfaces such as Ir(100) for which independent information on substrate structure is available, would clearly be of interest and are planned.

Acknowledgment. R.G. gratefully acknowledges the Ministry of Education and Science (Spain) and U.S.I.A. for a MEC/Fulbright Fellowship. This work is supported in part by the U.S. National Science Foundation.

References and Notes

(1) (a) Somorjai, G. A.; Van Hove, M. A. *Prog. Surf. Sci.* **1989**, *30*, 201. (b) Titmuss, S.; Wander, A.; King, D. A. *Chem. Rev.* **1996**, *96*, 1291. (c) Thiel, P. A.; Estrup, P. J. In *CRC Handbook of Surface Imaging and Visualization*; Hubbard, A. T., Ed.; CRC Press: Boca Raton, FL, 1993.

(2) (a) Weaver, M. J.; Gao, X. *Annu. Rev. Phys. Chem.* **1993**, *44*, 459. (b) Weaver, M. J. *J. Phys. Chem.* **1996**, *100*, 13079.

(3) Kolb, D. M. *Prog. Surf. Sci.* **1996**, *51*, 109.

(4) Kolb, D. M. In *Structure of Electrified Interfaces*; Lipkowski, J., Ross, P. N., Eds.; VCH Publishers: New York, 1993; Chapter 3.

(5) Nichols, R. J. In *Adsorption of Molecules at Electrodes*; Lipkowski, J., Ross, P. N., Eds.; VCH Publishers: New York, 1992; Chapter 7.

(6) Iwasita, T.; Nart, F. C. In *Advances in Electrochemical Science and Engineering*; Gerischer, H., Tobias, C. W., Eds.; VCH Publishers: New York, 1995; Vol. 4, p 123.

(7) Weaver, M. J.; Zou, S. In *Advances in Spectroscopy*; Clark, R. J. H., Hester, R. E., Eds.; Wiley: New York, 1998; Vol. 26, Chapter 5.

(8) Chang, S.-C.; Weaver, M. J. *J. Phys. Chem.* **1991**, *95*, 5391.

(9) Chang, S.-C.; Weaver, M. J. *Surf. Sci.* **1990**, *238*, 142.

(10) Villegas, I.; Weaver, M. J. *J. Chem. Phys.* **1994**, *101*, 1648.

(11) Villegas, I.; Weaver, M. J. *J. Phys. Chem. B* **1997**, *101*, 10166.

(12) Wagner, F. T. In ref 4, Chapter 9.

(13) (a) Gómez, R.; Weaver, M. J. *Langmuir* **1998**, *14*, 2525. (b) Gómez, R.; Weaver, M. J. Manuscript in preparation.
(14) Gómez, R.; Weaver, M. J. *J. Electroanal. Chem.* **1997**, *435*, 205.
(15) (a) Zou, S.; Gómez, R.; Weaver, M. J. *Surf. Sci*. **1998**, *399*, 270. (b) Gómez, R.; Zou, S.; Weaver, M. J., to be published.
(16) (a) Kisters, G.; Chen, J. G.; Lehwald, S.; Ibach, H. *Surf. Sci.* **1991**, *245*, 65. (b) Martin, R.; Gardner, P.; Nalezinski, R.; Tüshaus, M.; Bradshaw, A. M. *J. Electron Spectrosc. Relat. Phenom*. **1993**, *64/65*, 619.
(17) Gardner, P.; Martin, R.; Nalezinski, R.; Lamont, C. L. A.; Weaver, M. J.; Bradshaw, A. M. *J. Chem. Soc., Faraday Trans*. **1995**, *91*, 3575.
(18) (a) Gardner, P.; Martin, R.; Tüshaus, M.; Bradshaw, A. M. *J. Electroanal. Spectrosc. Relat. Phenom*. **1990**, *54/55*, 619*; Surf. Sci*. **1993**, *269/270*, 135.
(19) Gardner, P.; Tüshaus, M.; Martin, R.; Bradshaw, A. M. *Surf. Sci*. **1990**, *240*, 112.
(20) Clavilier, J.; Faure, R.; Guinet, G.; Durand, R. *J. Electroanal. Chem*. **1980**, *107*, 205.
(21) (a) Chang, S.-C.; Weaver, M. J. *J. Phys. Chem*. **1990**, *94*, 5095. (b) Villegas, I.; Weaver, M. J. *J. Electroanal. Chem*. **1994**, *373*, 245.
(22) (a) Rodes, A.; Gómez, R.; Perez, J. M.; Feliu, J. M.; Aldaz, A. *Electrochim. Acta* **1996**, *41*, 729. (b) Rodes, A.; Gómez, R.; Orts, J. M.; Feliu, J. M.; Perez, J. M.; Aldaz, A. A. *Langmuir* **1995**, *1*, 3549. (c) Gómez, R.; Rhodes, A.; Perez, J. M.; Feliu, J. M. *J. Electroanal. Chem*. **1995**, *393*, 123. (d) Gómez, R.; Rodes, A.; Orts, J. M.; Feliu, J. M.; Perez, J. M. *Surf. Sci*. **1995**, *342*, L1104. (e) Villegas, I.; Gómez, R.; Weaver, M. J. *J. Phys. Chem.* **1995**, *99*, 14832.
(23) Chang, S.-C.; Weaver, M. J. *J. Chem. Phys*. **1990**, *92*, 4582.
(24) Corrigan, D. S.; Weaver, M. J. *J. Phys. Chem*. **1986**, *90*, 5300.
(25) (a) Motoo, S.; Furuya, N. *J. Electroanal. Chem*. **1984**, *181*, 301. (b) Motoo, S.; Furuya, N. *J. Electroanal. Chem*. **1984**, *167*, 309. (c) Furuya, N.; Koide, S. *Surf. Sci*. **1990**, *226*, 221.
(26) Gómez, R.; Weaver, M. J., to be published.
(27) (a) Iwasita, T.; Nart, F. C.; Rodes, A.; Pastor, E.; Weber, M. *Electrochim. Acta* **1995**, *40*, 53. (b) Nart, F. C.; Iwasita, T.; Weber, M. *Electrochim. Acta* **1994**, *39*, 2093.
(28) Weaver, M. J.; Chang, S.-C.; Leung, L.-W. H.; Jiang, X.; Rubel, M.; Szklarzyk, M.; Wieckowski, A. *J. Electroanal. Chem*. **1992**, *327*, 247.
(29) Chang, S.-C.; Ho, Y.; Weaver, M. J. *J. Electrochem. Soc*. **1992**, *139*, 147.
(30) (a) Gómez, R.; Rodes, A.; Perez, J. M.; Feliu, J. M.; Aldaz, A. *Surf. Sci*. **1995**, *327*, 202. (b) Gómez, R.; Rodes, A.; Perez, J. M.; Feliu, J. M.; Aldaz, A. *Surf. Sci.* **1995**, *344*, 85.
(31) Gómez, R.; Feliu, J. M.; Aldaz, A.; Weaver, M. J. *Surf. Sci*., in press.
(32) Clavilier, J.; Albalat, R.; Gómez, R.; Orts, J. M.; Feliu, J. M. *J. Electroanal. Chem*. **1993**, *360*, 325.
(33) (a) Chang, S.-C.; Weaver, M. J. *Surf. Sci*. **1990**, *230*, 222. (b) Chang, S.-C.; Weaver, M. J. *J. Electroanal. Chem*. **1990**, *285*, 263.
(34) Chang, S.-C.; Roth, J. D.; Weaver, M. J. *Surf. Sci*. **1991**, *244*, 113.
(35) (a) Asensio, M. C.; Woodruff, D. P.; Robinson, A. W.; Schindler, K.-M.; Gardner, P.; Ricken, D.; Bradshaw, A. M.; Conesa, J. C.; Gonzalez-Elipe, A. R. *Chem. Phys. Lett*. **1992**, *192*, 259. (b) Aminpirooz, S.; Schmalz, A.; Becker, L.; Haase, J. *Phys. Rev. B* **1992**, *45*, 6337. (c) Mapledoram, L. D.; Wander, A.; King, D. A. *Chem. Phys. Lett*. **1993**, *208*, 409. (d) Schindler, K.-M.; Hofmann, Ph.; Weiss, K.-U.; Dippel, R.; Gardner, P.; Fritzsche, V.; Bradshaw, A. M.; Woodruff, D. P.; Davila, M. E.; Asensio, M. C.; Consesa, J. C.; Gonzalez-Elipe, A. R. *J. Electron Spectrosc. Relat. Phenom*. **1993**, *64/65*, 75.
(36) Lyons, K. J.; Xie, J.; Mitchell, W. J.; Weinberg, W. H. *Surf. Sci*. **1995**, *325*, 85. (b) Lauterbach, J.; Boyle, R. W.; Schick, Mitchell, W. J.; Meng, B.; Weinberg, W. H. *Surf. Sci*. **1996**, *350*, 32. (c) Marinov, T. S.; Chakarov, *Surf. Sci*. **1989**, *217*, 65.
(37) Jiang, X.; Chang, S.-C.; Weaver, M. J. *J. Phys. Chem*. **1991**, *95*, 7453.
(38) Lambert, D. K. *Electrochim Acta* **1996**, *41*, 661.
(39) Weaver, M. J. *Appl. Surf. Sci*. **1993**, *67*, 147.
(40) (a) Chang, S.-C.; Jiang, X.; Roth, J. D.; Weaver, M. J. *J. Phys. Chem*. **1991**, *95*, 5378. (b) Jiang, X.; Weaver, M. J. *Surf. Sci*. **1992**, *275*, 237.
(41) (a) Trasatti, S. *J. Electroanal. Chem*. **1983**, *150*, 1; **1982**, *139*, 1. (b) Trasatti, S. *Electrochim. Acta* **1983**, *28*, 1083. (c) Trasatti, S. *Electrochim. Acta* **1990**, *35*, 269.
(42) This value is an average of the two (disparate) estimates of E_k in the literature (cf. ref 8; see ref 12 for an enlightening discussion of the physical issues involved).
(43) Nieuwenhuys, B. E.; Sachtler, W. M. H. *Surf. Sci*. **1974**, *45*, 513.
(44) Nieuwenhuys, B. E. *Surf. Sci*. **1981**, *105*, 505.
(45) (a) Kanski, J.; Rhodin, T. N. *Surf. Sci*. **1977**, *65*, 63. (b) Zhdan, P. A.; Boreskov, G. K.; Boronin, A. I.; Scheelin, A. P.; Engelhoff, Jr., W. F.; Weinberg, W. H. *J. Catal*. **1979**, *60*, 93. (c) Ibbertson, D. E.; Wittrig, T. S.; Weinberg, W. H. *Surf. Sci*. **1981**, *110*, 294. (d) Davis, J. E.; Kapeboom, S. G.; Nolan, P. D.; Mullins, C. B. *J. Chem. Phys*. **1996**, *105*, 8362.
(46) Zou, S.; Gómez, R.; Weaver, M. J. *Langmuir* **1997**, *13*, 6713.
(47) Rodes, A.; Gómez, R.; Orts, J. M.; Feliu, J. M.; Aldaz, A. *J. Electroanal. Chem*. **1993**, *359*, 315.
(48) Attard, G., private communication, Sept 1997.
(49) For reviews, see: (a) White, J. M.; Akhter, S. *CRC Crit. Rev. Solid State Mater. Sci.* **1988**, *14*, 131. (b) White, J. M. *J. Phys. Chem*. **1983**, *87*, 915.
(50) (a) Kim, Y.; Peebles, H. C.; White, J. M. *Surf. Sci*. **1982**, *114*, 363. (b) Peebles, D. E.; Peebles, H. C.; White, J. M. *Surf. Sci*. **1984**, *136*, 463.
(51) (a) Richter, L. J.; Gurney, B. A.; Ho, W. *J. Chem. Phys*. **1987**, *86*, 477. (b) Richter, L. J.; Germer, T. A.; Ho, W. *Surf. Sci*. **1988**, *195*, L182.
(52) Hoge, D.; Tüshaus, M.; Bradshaw, A. M. *Surf. Sci*. **1988**, *207*, L935.
(53) Angerstein-Kozlowska, H.; Klinger, J.; Conway, B. E. *J. Electroanal. Chem*. **1977**, *75*, 45.
(54) Gardner, P.; Martin, R.; Tüshaus, M.; Bradshaw, A. M. *J. Electron Spectrosc. Relat. Phenom*. **1990**, *54/55*, 619.
(55) Marković, N. M.; Grgur, B. N.; Lucas, C. A.; Ross, P. N. *Surf. Sci*. **1997**, *384*, L805.